Scientia Iranica B (2023) 30(5), 1572–1586

SCIENTIA IRANICA

Sharif University of Technology
Scientia Iranica
Transactions B: Mechanical Engineering
http://scientiairanica.sharif.edu

Mathematical modeling of Williamson's model for blood flow inside permeable multiple stenosed arteries with electro-osmosis

S. Nadeem, J. Abbas Haider, and S. Akhtar*

Department of Mathematics, Quaid-i-Azam University 45320, Islamabad 44000, Pakistan.

Received 25 January 2022; received in revised form 22 May 2022; accepted 16 April 2023

KEYWORDS
Williamson's fluid model;
Joule heating effect;
Homotopy perturbation method;
Multiple stenoses;
Electro-osmotic effect.

Abstract. This study focuses on an artery with multiple stenoses, emphasizing the electro-osmotic effects. The artery's walls are porous, and slip boundary effects are present. Blood flow problems are better modeled with a slip and porous border. It is examined extensively due to the wide range of applications in the medical field, especially in diagnosing drug delivery and handling cellular irregularities. In this paper, we have visualized the non-Newtonian behavior of blood by using viscoelastic fluids as Williamson's fluid model. A mathematical model for an incompressible fluid is created, and the mathematical issue is then transformed into its dimensionless form by applying limitations in the case of mild multiple stenoses. The partial differential equations for the velocity and temperature profiles can be found when the problem is put into a dimensionless form. Analytical solutions of the resulting system are calculated with the help of the Homotopy Perturbation Method (HPM). The visual representation of analytically obtained solutions is investigated for both symmetric and non-symmetric geometries of stenosis. For varied values of flow rate Q and electro-osmotic parameter m, the streamlines are examined in detail.

1. Introduction

Blood flow via narrowed, stenosed arteries has recently attracted the attention of researchers. This is because blood flow through arteries poses serious health risks and is a leading cause of mortality and morbidity in industrialized countries. The narrowing of an artery, known as stenosis, may occur due to a significant buildup of plaque and can result in a significant decrease in blood flow. Plaque pieces, called emboli, could break off and get stuck in an artery further downstream, blocking it. The study of deformation and blood flow through stenosed arteries can be modeled as a Newtonian flow only in large arteries where the shear rate is greater than 100 per second. Blood is not a solid material; it is made up of a large number of cells like platelets, red blood cells, white blood cells, and different types of salts. Blood is considered a heterogenous mixture because it is a mixture of plasma and solid material (platelets, red blood cells, white blood cells). Blood is treated as a multiple-phase flow. In the case of small arteries, blood does not heed the law of Newtonian fluid. In the small arteries, blood has a non-Newtonian flow behavior. Eventually, the flow develops due to the electric field [1]. Electro-

*. *Corresponding author.*
E-mail address: sakhtar@math.qau.edu.pk (S. Akhtar)

doi: 10.24200/sci.2023.59837.6457

osmosis has several applications in the medical arena, including the treatment of disorders such as cellular abnormalities and sickle cells, as well as the administration of medications via the use of diagnostic kits. [2]. The extensive investigation of capillary electrokinetics as well as numerous micro-chip technologies, are discussed [3]. Wu and Papadopoulos [4] have proposed a mathematical model that compares the electro-kinetic fluxes in cylindrical and annular shapes. Yang et al. [5] conducted a mathematical analysis of the flow between two parallel plates created electrokinetically. Zhao and Yang [6] have mathematically investigated the two-dimensional flow of a power law fluid using electro-osmosis to get the desired result. A new interpretation of non-Newtonian fluid flow in tiny-length tubes was provided by Tang et al. [7], who was among the first to do so. When Liu et al. [8] used the Jeffery fluid model to simulate microslit channel flow, they were able to analyze the flow using an electrokinetic process. In a mathematical study conducted by Nadeem et al. [9], the Electro-Osmotic Flow (EOF) of the Bingham plastic fluid via a micro-length tube was investigated. Recent study publications that interpret the EOF phenomena are cited by Narla and Tripathi [10] Tripathi et al. [11] Akram et al. [12] and Saleem et al. [13] among others.

The presence of stenosis in the blood vessels results in a limitation of hemodynamics throughout the sick arteries in the body. In some instances, such arteries may have more than one stenosis due to specific disorders. The investigation of flow across such a large number of stenosed arteries has also recently piqued the attention of experts. In his PhD dissertation, Dr. Ponalagusamy [14] published the first study on the flow over stenosed arteries, which was the first of its kind. This vascular study of moderate stenosis includes coverage of stenosis of different forms as well as other conditions. [15]. A non-Newtonian fluid flow over a channel with numerous stenosis has been described by Varshney et al. [16], who offered mathematical research on the flow. In a previous study, Nadeem and Ijaz [17] investigated blood flow via numerous stenosed tubes by treating blood as a Casson fluid. When Akbar et al. [18] looked at the blood flow over a multiple-stenosed tube with varied fluid characteristics, they came up with some interesting results. When different non-Newtonian fluid models are considered, we provide a mathematical model for the blood flow through such diseased multiple stenosed arteries. [19–23].

Riaz et al. investigated a new model of entropy production effects evaluated in the Cu-blood flow of a nanofluid under the influence of ciliary-oriented motion [24]. The study presents a thermal analysis of Cu-CuO/blood nanofluids flow in an asymmetric microchannel propagating with wave velocity [25]. Specifically, the electro-osmotic Couette-Poiseuille flow of power law Al_2O_3-PVC nanofluid through a channel with an upper wall moving with constant velocity is described in the present work [26]. Researchers at the University of California, Berkeley, studied the effects of magnetized Williamson's nanofluid flow on parallel rotating plates under squeezing impacts in the presence of gyrotactic micro-organisms [27]. A non-Newtonian fluid does not follow Newton's law of viscosity, which says that viscosity stays the same no matter how much force is put on it. When a force is put on a fluid that is not a Newtonian fluid, the viscosity can change, making the fluid more liquid or more solid. For example, when you shake ketchup, it gets runnier, so it is not a Newtonian fluid. Non-Newtonian fluids include many saline solutions, molten polymers, and everyday things like custard, toothpaste, starch suspensions, corn starch, paint, blood, melted butter, and shampoo [28]. Williamson's fluid model describes the flow of shear-thinning non-Newtonian fluids. Williamson [29] first proposed this hypothesis in 1929 and provided experimental evidence to support it. For a stationary (zero fluid motion) Williamson's fluid model, the effective viscosity should decrease forever with increasing shear rate, which is nothing more than an infinite viscosity at zero fluid motion and a nil viscosity as the shear rate approaches infinity. In [30,31], a few recent investigations into Williamson's fluid are discussed in detail. Khan et al. [32] studied Williamson's fluid flow in a lab with chemically reactive species using scaling conversion and Homotopy analysis. The Homotopy Perturbation Method (HPM) is a semi-analytical method for solving linear and nonlinear ordinary and partial differential equations, and it is widely used in the industry. This approach may also solve a system of linked linear and nonlinear differential equations [33–37]. The same technique was also applied to more complicated results to solve the designed blood flow problem.

The study of parallel nonlinear radiation, magnetohydrodynamic effects in Marangoni convection nanofluids, and spatially dependent heat sources are discussed [38]. It involves the investigation of the influence of velocity slip on the hydromagnetic peristaltic flow of a Casson fluid and the heat transfer via an asymmetric channel fluid packed in a porous medium. Another swarm intelligence optimization approach known as the Artificial Coronary Circulation System is suggested in the references. The expansion of the human heart's coronary arteries (veins) is simulated using this optimization approach. It is shown in this article that the lattice Boltzmann technique may be used to model two-dimensional incompressible viscous flow in open and closed microchannels (vessels). The main goal of the current research is to figure out how blood moves through blood vessels physically [39–47]. The number of methods used to determine the blood flow behavior,

analytical and numerical, investigation of the good results for visualizing the behavior of the stenosis and diseased arteries. Using User-Defined Function (UDF) in Fluent, the Finite Volume Method (FVM) approach is used to simulate blood flow dynamics inside stenosis arteries based on the non-Newtonian Sisko model [48]. The magnetohydrodynamic blood flow research in stenotic coronary arteries was investigated using the lattice Boltzmann technique with the assistance of the finite element method in stenotic coronary arteries [49]. Several studies have compared the differences between Computational Fluid Dynamics (CFD) and Fluid Solid Interaction (FSI) simulations; however, as demonstrated, there is still debate about whether the most realistic technique, namely calculating WSS-dependent variables, is necessary and the results are frequently contradictory. This paper compares the results of CFD and FSI simulations in an idealized stenotic coronary artery with 50% stenosis [50]. Although solid numerical techniques with the amazing computational power of computers are available to find numerical solutions with great accuracy, the analytical solutions cannot be ignored. The benefit of an analytical solution is that you can understand the physics of the solution deeply and clearly and help check the validity of numerical solutions [51–56].

Carotid arteries are parried blood vessels arising from the arch of the aorta above the heart [57]. They deliver oxygenated blood to the face, head, and brain [58]. The external carotid artery supplies blood to the head and face, and the internal carotid artery conveys supply to the brain. Carotid arteries damage the vessel wall's inner layers due to the blood's narrow path [59]. Causes of 10–20% ischemic (when the blood supply towards the heart is not enough as required) strokes. Atherosclerotic plaque can send clots to the retina's blood vessels, causing transient or permanent visual loss [60]. Environmental risk factors cause stenosis, such as smoking, high cholesterol, high blood pressure, diabetes/high blood sugar, obesity, and injuries to vessel walls [61].

In addition, we have also used the effect of electro-osmotic in this paper. The charged colloidal particles move under the influence of an electric field during electrophoresis. If electrophoresis is avoided by maintaining the particles stationary, the dispersion medium will move under the influence of an electric field. This movement of dispersion medium under the influence of an electric field is called EOF. It is also easy to define that it is the movement of separation of mixture components through the silica capillary due to zeta potential at the solvent silica inference. The zeta potential is the potential difference existing between the surface of solid particles immersed in a conducting liquid and the bulk of the liquid. Our new contribution to this work is that we have used Williamson's fluid model to study the non-Newtonian behavior of the blood. After developing the model, we have non-dimensionalized it to simplify this complex problem. This is the first research article that highlights the physics of the non-Newtonian Williamson' fluid model for blood flow inside a multiple stenosed artery under electro-osmotic effects. A permeable artery having multiple stenoses is considered for this non-Newtonian blood flow problem. The solutions obtained by the HPM are approximate and not exact. However, these solutions satisfy both the boundary conditions and the effect of multiple stenoses. The graphs of these mathematical solutions also meet the requirements for speed and temperature at the edges.

2. Mathematical model

In this model, we considered the blood flow in the tapered channel. The rectangular coordinate system (r, z) is considered such that the length of the channel is along the z-axis and the width of the channel is along the r-axis. The flow of Williamson's fluid inside the wavy channel is caused by the sinusoidal wave propagating with speed s along the deformable walls of the channel. We studied the combined effect of electro-osmotic and multiple stenoses and analyzed the blood's non-Newtonian behavior using Williamson's fluid tensor with cylindrical coordinates (r, z).

Consider the geometry of the multiple stenoses [62] as Figure 1 given.

Multi-stenosis wall geometry in dimensional form is expressed as follows [63]:

$$\eta(z) = \begin{cases} R\left[1-K\left\{s_l^{n-1}(z-d_l)-(z-d_l)^n\right\}\right], d_l \leq z \leq d_l \\ R, \quad \text{otherwise} \end{cases}. \quad (1)$$

Here we define the value of:

$$K = \frac{s_l^*}{Rs_l^n}\frac{n^{\frac{1}{n-1}}}{n-1}. \quad (2)$$

The governing equations for blood flow with multiple stenoses [63] and Williamson's fluid model are written as follows:

$$\frac{\partial v}{\partial r} + \frac{v}{r} + \frac{\partial u}{\partial z} = 0, \quad (3)$$

$$\rho\left[v\frac{\partial v}{\partial r} + u\frac{\partial v}{\partial z}\right] = -\frac{\partial p}{\partial r} + \frac{1}{r}\frac{\partial}{\partial r}(rS_{rr}) + \frac{\partial}{\partial z}(S_{rz}), \quad (4)$$

$$\rho\left[v\frac{\partial u}{\partial r} + u\frac{\partial u}{\partial z}\right] = -\frac{\partial p}{\partial z} + \frac{1}{r}\frac{\partial}{\partial r}(rS_{rz}) + \frac{\partial}{\partial z}(S_{zz}) + \rho_e E_z, \quad (5)$$

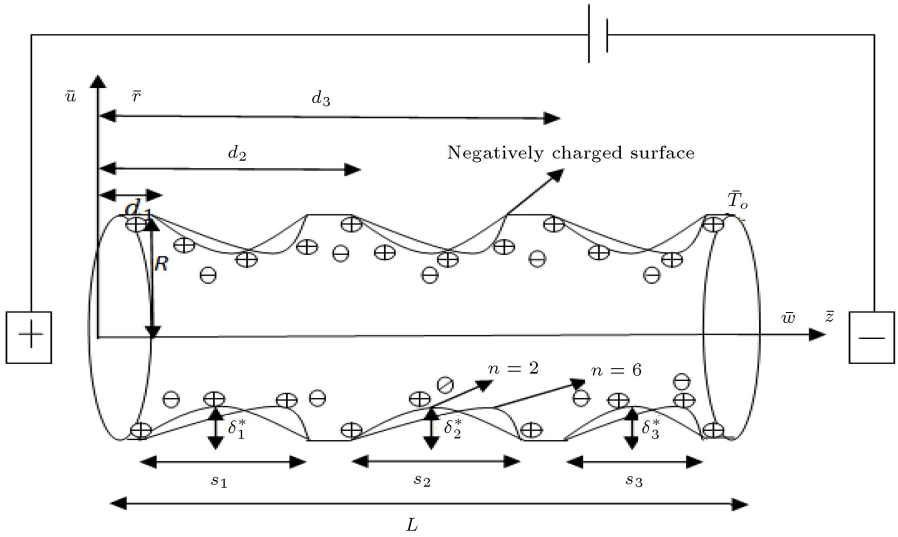

Figure 1. Geometry of the problem.

$$\rho C_p \left[v\frac{\partial T}{\partial r} + u\frac{\partial T}{\partial z} \right] = S_{rr}\frac{\partial v}{\partial r} + S_{rz}\frac{\partial u}{\partial r} + S_{zr}\frac{\partial v}{\partial z} + S_{zz}\frac{\partial u}{\partial z} + k\left[\frac{\partial^2 T}{\partial r^2} + \frac{1}{r}\frac{\partial v}{\partial z} + \frac{\partial^2 T}{\partial z^2} \right] + S^*. \quad (6)$$

Here we consider the non-Newtonian fluid model to discuss the nature of blood. The considered extra stress tensor for Williamson's fluid model [32] is provided as:

$$S_{ij} = \eta_0(1 + \Gamma|\dot{\gamma}_{ij}|)\dot{\gamma}_{ij}, \quad (7)$$

here,

$$\dot{\gamma}_{ij} = \frac{\partial v_i}{\partial x_j} + \frac{\partial v_j}{\partial x_i}, \quad (8)$$

$$|\dot{\gamma}_{ij}| = \sqrt{\left(\frac{1}{2}\sum_i \sum_j \gamma_{ij} \right)}. \quad (9)$$

In the above equation S^* has the value of $S^* = I_e^2\sigma_e$ where $I_e = \frac{E_Z}{\sigma_e}$ [64]. The channel is filled with blood taken as an ionic solution, modified by an external electric field. Electrostatics theory says this about the Poisson-Boltzmann equation, which describes how the electric potential is spread out in a symmetric binary electrolyte solution:

$$\Delta\phi = \frac{\rho_e}{E}. \quad (10)$$

We choose the value of $\rho_e = ez^*n^+ - ez^*n^-$, where e is electric charge, z^* charge balance, n^+ is the cation density, and n^- is the anion density:

$$n^{\pm} = n_0 e^{\left(\frac{ez^*\phi}{K_B T^*}\right)}. \quad (11)$$

By using the value of ρ_e and above equation, we have:

$$\frac{1}{r}\frac{\partial}{\partial r}\left(r\frac{\partial\phi}{\partial r} \right) = \frac{2n_0e^2z^{*2}\phi}{K_BT}, \quad (12)$$

$$\frac{1}{r}\frac{\partial}{\partial r}\left(r\frac{\partial\bar{\phi}}{\partial r} \right) = m^2\bar{\phi}. \quad (13)$$

Here $\text{Sinh}\left(\frac{ez^*\phi}{K_BT^*}\right) \approx \left(\frac{ez^*\phi}{K_BT^*}\right)$ and square of the electro-osmotic parameter is $m^2 = \frac{2n_0e^2z^{*2}R^2}{K_BT^*E}$. By using Mathematica software, we find the solution of Eq. (13):

$$\phi = \frac{BesselI[0, m*\bar{r}]}{BesselI[0, m*\bar{r}]}. \quad (14)$$

Eq. (14) is the exact solution, which is found using these boundary conditions:

$$\bar{\phi} = 0 \text{ at } \bar{r} = 0 \text{ and } \bar{\phi}' = 1 \text{ at, } \bar{r} = \eta(z). \quad (15)$$

We introduce the following dimensionless variables:

$$\bar{v} = \frac{L}{\delta_l^* U_0}v, \quad \bar{u} = \frac{1}{U_0}u, \quad \bar{r} = \frac{r}{R}, \quad \bar{z} = \frac{1}{s_l}z,$$

$$\bar{\eta}(z) = \frac{\eta(z)}{R}, \quad \bar{p} = \frac{R^2p}{U_0s_l\mu_f}, \quad \delta_l^* = \frac{\delta_l}{R}, \quad h_l = \frac{d_l}{s_l},$$

$$\bar{S}_{rr} = \frac{R}{U_0\mu_f}S_{rr}, \quad \bar{S}_{rz} = \frac{R}{U_0\mu_f}S_{rz}, \quad \bar{S}_{zz} = \frac{R}{U_0\mu_f}S_{zz},$$

$$S = \frac{E_z^2R^2}{\sigma_e\bar{T}_0k}, \quad U_{HS} = \frac{E_zE\xi}{U_0\mu_f}, \quad \bar{\phi} = \frac{\phi}{\xi}, \quad W_e = \frac{\Gamma U_0}{R},$$

$$\dot{\gamma}_{ij} = \frac{R}{U_0}\dot{\gamma}_{ij}, \quad Br = \frac{\mu_fU_0^2}{k_f\bar{T}_0}, \quad \theta = \frac{\bar{T} - \bar{T}_0}{\bar{T}_0}. \quad (16)$$

Employing Eq. (16) on Eqs. (3)–(7), we get the following dimensionless equations. After applying limitations

in the case of mild multiple stenoses [63]:

$$\delta_l^* = \frac{\delta_l}{R} \ll 1, \frac{Rn^{\frac{1}{n}} - 1}{s_l} \sim o1. \tag{17}$$

Eqs. (3)–(7) become:

$$\frac{\partial \bar{v}}{\partial \bar{r}} + \frac{\bar{v}}{\bar{r}} + \frac{\partial \bar{u}}{\partial \bar{z}} = 0, \tag{18}$$

$$\frac{\partial \bar{p}}{\partial \bar{r}} = 0, \tag{19}$$

$$-\frac{\partial \bar{p}}{\partial \bar{z}} + \frac{1}{\bar{r}}\frac{\partial}{\partial \bar{r}}(\bar{r}\bar{S}_{rz}) + U_{HS}m^2\bar{\phi} = 0, \tag{20}$$

$$Br\bar{S}_{rz}\frac{\partial \bar{u}}{\partial \bar{r}} + \frac{\partial^2 \theta}{\partial \bar{r}^2} + \frac{1}{\bar{r}}\frac{\partial \theta}{\partial \bar{r}} + S = 0. \tag{21}$$

Williamson's fluid model gives:

$$\bar{S}_{rr} = 2(1 + W_e|\dot{\gamma_{ij}}|)\frac{\partial \bar{v}}{\partial \bar{r}}, \tag{22}$$

$$\bar{S}_{rz} = 2(1 + W_e|\dot{\gamma_{ij}}|)\frac{\partial \bar{u}}{\partial \bar{r}}, \tag{23}$$

$$\bar{S}_{zz} = 2(1 + W_e|\dot{\gamma_{ij}}|)\frac{\partial \bar{u}}{\partial \bar{z}}, \tag{24}$$

$$\bar{S}_{rz} = \bar{S}_{zr} = (1 + W_e\frac{\partial \bar{u}}{\partial \bar{r}})\frac{\partial \bar{u}}{\partial \bar{r}}. \tag{25}$$

By using Eq. (25), Eqs. (20) and (21) become (after dropping the bars):

$$-\frac{\partial \bar{p}}{\partial \bar{z}} + \frac{1}{\bar{r}}\frac{\partial}{\partial \bar{r}}(\bar{r}\left((1 + W_e\frac{\partial \bar{u}}{\partial \bar{r}})\frac{\partial \bar{u}}{\partial \bar{r}}\right)) + U_{HS}m^2\bar{\phi} = 0, \tag{26}$$

$$Br\left(\left(1 + W_e\frac{\partial \bar{u}}{\partial \bar{r}}\right)\frac{\partial \bar{u}}{\partial \bar{r}}\right)\frac{\partial \bar{u}}{\partial \bar{r}} + \frac{\partial^2 \theta}{\partial \bar{r}^2} + \frac{1}{\bar{r}}\frac{\partial \theta}{\partial \bar{r}} + S = 0. \tag{27}$$

Here the dimensionless numbers Br, W_e are Brinkman number and Wassenberg number. On velocity and temperature, the non-dimensional boundary conditions [65] are:

$$\frac{\partial \bar{u}}{\partial \bar{r}} = 0 \quad \text{at} \quad \bar{r} = 0, \tag{28}$$

$$u = u_B \quad \text{at} \quad r = \eta, \quad \frac{\partial \bar{u}}{\partial \bar{r}} = \frac{\alpha}{\sqrt{D_\alpha}}(\bar{u}_B - \bar{u}_{porous}),$$

$$\bar{u}_{porous} = D_\alpha\left(\frac{\partial \bar{p}}{\partial \bar{z}}\right),$$

$$\frac{\partial \theta}{\partial \bar{r}} = 0 \quad \text{at} \quad \bar{r} = 0 \quad \text{and} \quad \theta = 0 \quad \text{at} \quad \bar{r} = \eta. \tag{29}$$

The above governing third-degree differential Eqs. (26) and (27) and slip boundary conditions are highly non-linear, so we cannot find their exact solutions using Mathematica software, so we used approximate solutions for these governing equations. We used the HPM to find the approximate solution. The non-slip boundary conditions are linear and easily solvable.

3. Solution of the problem

The solution of the non-linear differential Eqs. (26) and (27) can be obtained using HPM with slip boundary conditions:

$$H(\bar{u}, q) = (1 - q)(L(\bar{u}) - L(u_0)) + q(L(\bar{u}) + N + f(z)), \tag{30}$$

where q, L, u_0 and N are called embedding parameter, linear operator, initial guess, and non-linear operator ($q \in [0, 1]$), respectively.

In the case of Eq. (26):

$$L = \frac{\partial^2 \bar{u}}{\partial \bar{r}^2} + \frac{1}{r}\frac{\partial \bar{u}}{\partial \bar{r}}, u_0 = \bar{u}_B + \frac{r^2 - \eta^2}{2}$$

$$N = \frac{W_e}{\bar{r}}\left(\frac{\partial \bar{u}}{\partial \bar{r}}\right)^2 + 2W_e\left(\frac{\partial \bar{u}}{\partial \bar{r}}\right)\left(\frac{\partial^2 \bar{u}}{\partial \bar{r}^2}\right) + U_{HS}m^2\frac{BesselI[0, m * \bar{r}]}{BesselI[0, m * \bar{r}]}, f(r, z) = \frac{\partial \bar{p}}{\partial \bar{z}}. \tag{31}$$

Applying Eq. (30) to Eq. (26), we have:

$$H(\bar{u}, q) = \begin{pmatrix} (1 - q)\left(\frac{\partial^2 \bar{u}}{\partial \bar{r}^2} + \frac{1}{r}\frac{\partial \bar{u}}{\partial \bar{r}} - L(u_0)\right) \\ q\left(\frac{\partial^2 \bar{u}}{\partial \bar{r}^2} + \frac{1}{r}\frac{\partial \bar{u}}{\partial \bar{r}} + \frac{W_e}{\bar{r}}\left(\frac{\partial \bar{u}}{\partial \bar{r}}\right)^2\right) + 2W_e\left(\frac{\partial \bar{u}}{\partial \bar{r}}\right)\left(\frac{\partial^2 \bar{u}}{\partial \bar{r}^2}\right) \\ +U_{HS}m^2\frac{BesselI[0, m*\bar{r}]}{BesselI[0, m*\bar{r}]} - \frac{\partial \bar{p}}{\partial \bar{z}} \end{pmatrix} = 0, \tag{32}$$

$$H(\theta, q) = (1 - q)(L(\theta) - L(\theta_0)) + q(L(\theta) + N + f(r, z)), \tag{33}$$

q, L, θ_0, and N are called embedding parameter, linear operator, initial guess, and non-linear operator ($q \in [0, 1]$), respectively:

$$L = \frac{\partial^2 \theta}{\partial \bar{r}^2} + \frac{1}{r}\frac{\partial \theta}{\partial \bar{r}}, \quad u_0 = \bar{u}_B + \frac{r^2 - \eta^2}{2},$$

$$\theta_0 = \frac{r^2 - \eta^2}{2},$$

$$N = Br\left(\frac{\partial \bar{u}}{\partial \bar{r}}\right)^2 + BrW_e\left(\frac{\partial \bar{u}}{\partial \bar{r}}\right)^3 f(r, z) = S. \tag{34}$$

Applying Eq. (33) to Eq. (27), we have:

$$H(\theta,q)=\begin{pmatrix}(1-q)\left(\frac{\partial^2\theta}{\partial\bar{r}^2}+\frac{1}{r}\frac{\partial\theta}{\partial\bar{r}}-L(\theta_0)\right)\\ q\left(\frac{\partial^2\theta}{\partial\bar{r}^2}+\frac{1}{r}\frac{\partial\theta}{\partial\bar{r}}+Br\left(\frac{\partial\bar{u}}{\partial\bar{r}}\right)^2\right)+BrW_e\left(\frac{\partial\bar{u}}{\partial\bar{r}}\right)^3+S\end{pmatrix}. \quad (35)$$

Now we define the series of θ and $\bar{u}$:

$$\bar{u}(\bar{r},\bar{z})=\bar{u}_0+q\bar{u}_1+q^2\bar{u}_2+..., \quad (36)$$

$$\theta(\bar{r},\bar{z})=\theta_0+q\theta_1+q^2\theta_2+.... \quad (37)$$

By substituting the values of Eqs. (36) and (37) into Eqs. (32) and (35) and then comparing the order of embedding parameters, the approximate solution is obtained.

Zeroth order $O(q^0)$:

$$L(\bar{u})-L(\bar{u})=0, \quad (38)$$

$$L(\theta)-L(\theta)=0, \quad (39)$$

$$\frac{\partial\bar{u}_0}{\partial\bar{r}}=0 \ \text{ at } \ \bar{r}=0, \qquad u_0=\bar{u} \ \text{ at } \ \bar{r}=\eta,$$

$$\frac{\partial\theta_0}{\partial\bar{r}}=0 \ \text{ at } \ \bar{r}=0, \quad \theta_0=0 \ \text{ at } \ \bar{r}=\eta. \quad (40)$$

First order $O(q^1)$:

$$\frac{\partial^2\bar{u}_1}{\partial\bar{r}^2}+\frac{1}{r}\frac{\partial\bar{u}_1}{\partial\bar{r}}+2+3W_e\bar{r}+U_{HS}m^2\frac{BesselI[0,m*\bar{r}]}{BesselI[0,m*\eta]}-\frac{\partial\bar{p}}{\partial\bar{z}}=0, \quad (41)$$

$$\frac{\partial^2\theta_1}{\partial\bar{r}^2}+\frac{1}{r}\frac{\partial\theta_1}{\partial\bar{r}}-2+Br*\bar{r}^2BrW_e\bar{r}^3+S=0, \quad (42)$$

$$\frac{\partial\bar{u}_1}{\partial\bar{r}}=0 \ \text{ at } \ \bar{r}=0, \quad u_1=0 \ \text{ at } \ \bar{r}=\eta,$$

$$\frac{\partial\theta_1}{\partial\bar{r}}=0 \ \text{ at } \ \bar{r}=0, \quad \theta_1=0 \ \text{ at } \ \bar{r}=\eta. \quad (43)$$

Second order $O(q^2)$:

$$\frac{\partial^2\bar{u}_2}{\partial\bar{r}^2}+\frac{1}{r}\frac{\partial\bar{u}_2}{\partial\bar{r}}+4W_e\frac{\partial\bar{u}_1}{\partial\bar{r}}+2W_e\bar{r}\frac{\partial^2\bar{u}_1}{\partial\bar{r}^2}=0, \quad (44)$$

$$\frac{\partial^2\theta_2}{\partial\bar{r}^2}+\frac{1}{r}\frac{\partial\theta_2}{\partial\bar{r}}+2Br\frac{\partial\bar{u}_1}{\partial\bar{r}}\bar{r}+3BrW_e\bar{r}^2\frac{\partial\bar{u}_1}{\partial\bar{r}}=0, \quad (45)$$

$$\frac{\partial\bar{u}_2}{\partial\bar{r}}=0 \ \text{ at } \ \bar{r}=0, \quad u_2=0 \ \text{ at } \ \bar{r}=\eta,$$

$$\frac{\partial\theta_2}{\partial\bar{r}}=0 \ \text{ at } \ \bar{r}=0, \quad \theta_2=0 \ \text{ at } \ \bar{r}=\eta. \quad (46)$$

Using Mathematica software, we find the series up to three iterations and take the embedding parameter equal to 1.

The solution of Eqs. (41)–(45) by using the slip boundary conditions (40), (43), (46) obtained by Eqs. (47) and (48) are shown in Box I. Mathematica result for pressure gradient obtained by Eq. (49) as shown in Box II.

On the walls of the multiple stenosed shares, stress is defined as:

$$\bar{\tau}_{\bar{u}}=\frac{\partial\bar{u}}{\partial\bar{r}}|_{\bar{r}=\eta},$$

$$\bar{u}=\begin{pmatrix}\frac{1}{12}U_{HS}m^2\frac{BesselI[0,m*\bar{r}]}{BesselI[0,m*\eta]}\begin{pmatrix}-12D_\alpha\frac{\partial\bar{p}}{\partial\bar{z}}+12U_{HS}+\bar{r}^2(p(3-4\bar{r}W_e)+\\ 2W_e\bar{r}(2+3W_e\bar{r}))-3p\eta^2\\ \frac{-6\sqrt{D_\alpha}\eta(\frac{\partial\bar{p}}{\partial\bar{z}}-2pW_e\eta+2W_e\eta(1+2W_e\eta))}{\alpha}\end{pmatrix}\\ \frac{1}{9BesselI[0,m\eta]}mU_{HS}\left(\frac{9\sqrt{D_\alpha}(-1+2W_e\eta)BesselI[1,m\eta]}{\alpha}\right.\\ +mW_e\left(\bar{r}^3\left(2HypergeometricPFQ\left[\begin{matrix}\{\frac{3}{2},\frac{3}{2}\},\\ \{1,\frac{5}{2},\frac{5}{2}\},\end{matrix}\frac{m^2\bar{r}^2}{4}\right]\right.\right.\\ HypergeometricPFQ\left[\begin{matrix}\{\frac{3}{2},\frac{3}{2}\},\\ \{2,\frac{5}{2},\frac{5}{2}\},\end{matrix}\frac{m^2\bar{r}^2}{4}\right]\Big)\\ -\eta^3\left(2HypergeometricPFQ\left[\begin{matrix}\{\frac{3}{2},\frac{3}{2}\},\\ \{1,\frac{5}{2},\frac{5}{2}\},\end{matrix}\frac{m^2\eta^2}{4}\right]\right.\\ \left.\left.HypergeometricPFQ\left[\begin{matrix}\{\frac{3}{2},\frac{3}{2}\},\\ \{2,\frac{5}{2},\frac{5}{2}\},\end{matrix}\frac{m^2\eta^2}{4}\right]\right)\right)\end{pmatrix}, \quad (47)$$

$$\bar{Q}=2*\pi\int_0^\eta\bar{r}\bar{u}d\bar{r}. \quad (48)$$

Box I

$$\frac{\partial \bar{p}}{\partial \bar{z}} = \left(\frac{\begin{array}{l} (-4((4(-90Q\alpha BesselI[0,m\eta] + 90\pi U_{HS}\alpha\eta^2 BesselI[0,m\eta] + \\ 90\sqrt{D_\alpha}\pi W_e\eta^4 BesselI[0,m\eta] + 180\sqrt{D_\alpha}\pi {W_e}^2\eta^5 BesselI[0,m\eta] \\ -18\pi W_e\eta^5\alpha BesselI[0,m\eta] - 30\pi W_e\eta^6\alpha BesselI[0,m\eta] - \\ 180\sqrt{D_\alpha}\pi m U_{HS} BesselI[1,m\eta] + 360 W_e\sqrt{D_\alpha}\pi m\eta^2 U_{HS} BesselI[1,m\eta] + \\ 720\pi\alpha\eta^2 W_e U_{HS} BesselI[2,m\eta] + 360 m\pi\eta^2 W_e U_{HS} BesselI[3,m\eta] - \\ 180\pi U_{HS}\alpha\eta HypergeometricPFQ[\{\frac{1}{2}\},\{1,\frac{3}{2}\},\frac{m^2\eta^2}{4}] - \\ 120 m^2\pi\alpha W_e\eta^4 HypergeometricPFQ[\{\frac{3}{2}\},\{1,\frac{5}{2}\},\frac{m^2\eta^2}{4}] - \\ 5m^2\pi\alpha W_e\eta^4 HypergeometricPFQ[\{\frac{3}{2},\frac{3}{2}\},\{\frac{5}{2},\frac{5}{2},3\},\frac{m^2\eta^2}{4}] \end{array}}{(9\pi\eta^2(-40 D_\alpha\alpha + 20\sqrt{D_\alpha}\eta - 40 W_e\eta^2\sqrt{D_\alpha} - 5\alpha\eta^2 + 8 W_e\alpha\eta^3) BesselI[0,m\eta])} \right). \quad (49)$$

Box II

$$\bar{\tau}_{\bar{u}} = -\frac{1}{2}\eta\left(\frac{\partial \bar{p}}{\partial \bar{z}} - 2\frac{\partial \bar{p}}{\partial \bar{z}} W_e\eta(1+2W_e\eta)\right) + \frac{mU_{HS}(1-2W_e) BesselI[1,m\eta]}{BesselI[0,m\eta]}. \quad (50)$$

The solution of the temperature profile is defined by Eq. (51) as shown in Box III.

4. Results and discussion

Here, We have discussed the mathematical results graphically for velocity, shear stress, and temperature obtained by the HPM. HPM is a semi-analytical technique for solving linear, non-linear, and coupled partial and ordinary differential equations. Analytical solutions to the differential equations are much better because they give us the problem's physics and are easy to understand. Here we discuss the physical results of mathematical modeling graphically. In this section, we analyzed and discussed the effects of various physical parameters on dimensionless velocity, shear stress, temperature, and streamlines, respectively. This allows us to see the effect of electro-osmotic parameters on the velocity, temperature, axial pressure gradient, and streamlines.

In Figures 2a–2e, the velocity graph is shown for increasing values of various physical parameters. The effect of Darcy number is shown in Figure 2a. The Darcy number (Da) in fluid dynamics via porous media indicates the relative influence of the medium's permeability on its cross-sectional area, generally the diameter squared. The Darcy number is the ratio of the medium's permeability to the characteristic length. The characteristic length is constant for the channel, and here we discuss the porosity that depends upon the medium's permeability. With an increase in the medium's permeability, Darcy number is also increased, as shown in Figure 2a. We have obtained the conditions for velocity that we have obtained by using Mathematica software. At different parameters in the graph, we take the symmetric shape of the multiple stenoses at $n = 2$ and the non-symmetric shape of multiple stenoses at $n = 6$. The velocity at the center is

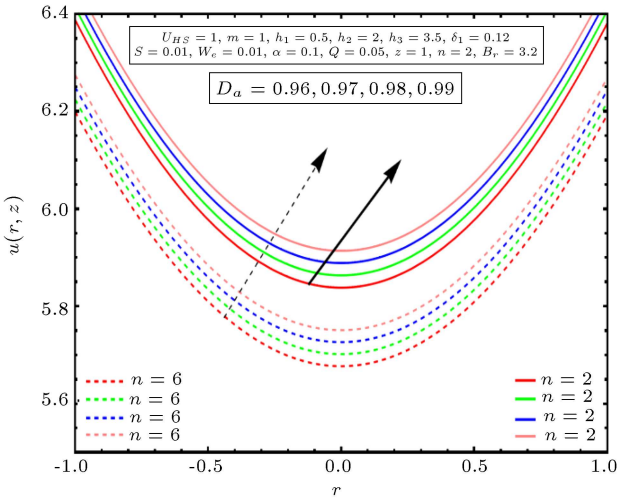

Figure 2a. Velocity along D_α.

$$\theta(\bar{r},\bar{z}) = \left(\begin{array}{l} \frac{1}{1200 m^2 BesselI[0,m\bar{r}]}(-4800 Br U_{HS} BesselI[0,m\bar{r}]) + (4800 Br U_{HS} + m^2(-75\bar{r}^2 \\ (Br(-1+\frac{\partial\bar{p}}{\partial\bar{z}})\bar{r}^2 + 4(-4+s)) + 24Br(8-3\frac{\partial\bar{p}}{\partial\bar{z}})\bar{r}^5 W_e + 100 Br {W_e}^2 + 300(-4+s)\eta^2 \\ +75Br(-1+\frac{\partial\bar{p}}{\partial\bar{z}})\eta^4 + 24Br m U_{HS}(100\bar{r} BesselI[1,m\bar{r}] - 100\eta BesselI[1,m\eta] \\ 3m^3 W_e(\bar{r}^5 HypergeometricPFQ[\{\frac{5}{2},\frac{5}{2}\},\{2,\frac{7}{2},\frac{7}{2}\},\frac{m^2\bar{r}^2}{4}] \\ -\eta^5 HypergeometricPFQ[\{\frac{5}{2},\frac{5}{2}\},\{2,\frac{7}{2},\frac{7}{2}\},\frac{m^2\bar{r}^2}{4}]))) \end{array} \right). \quad (51)$$

Box III

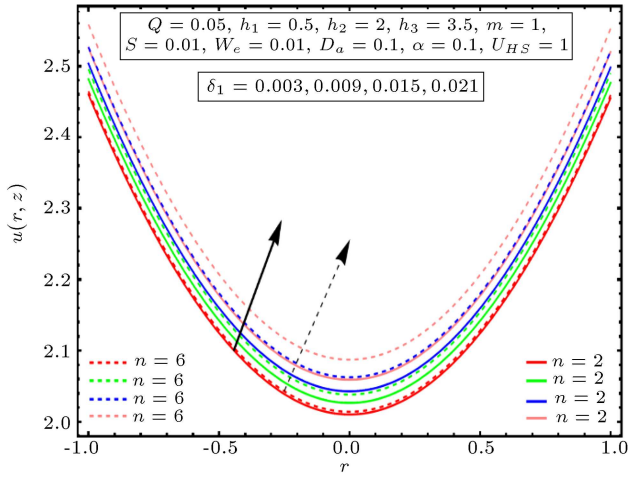

Figure 2b. Velocity along δ_l.

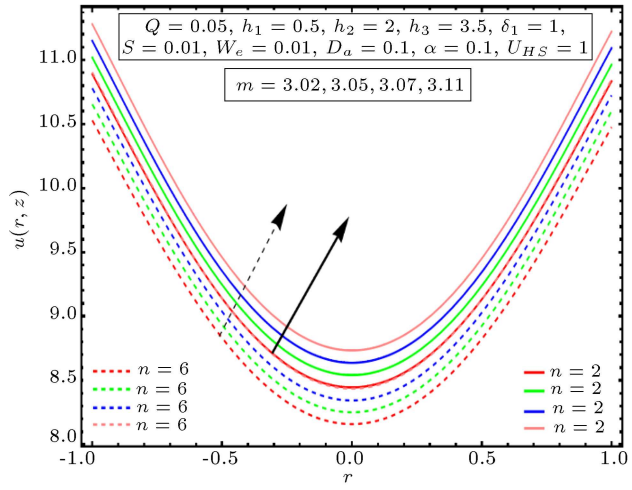

Figure 2c. Velocity along m.

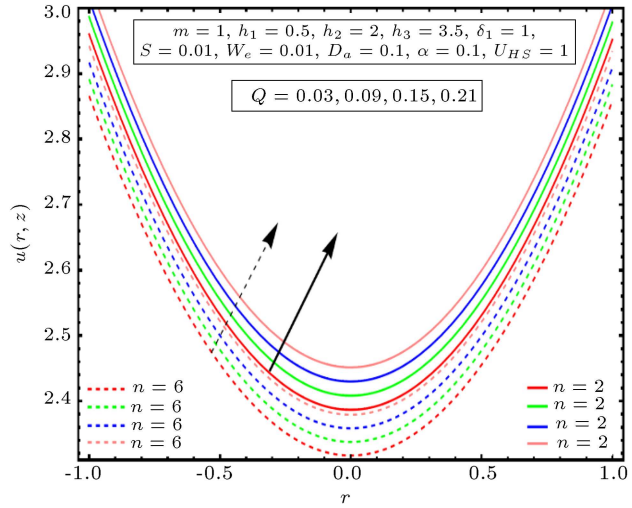

Figure 2d. Velocity along Q.

minimum, but the velocity increases towards the walls of the channel, and the velocity increases by increasing Darcy number. Figure 2b shows the behavior of the velocity graph for stenosis length (δ_l) at four different

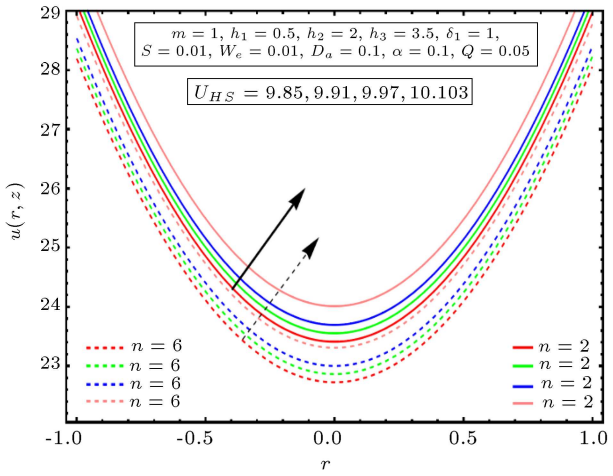

Figure 2e. Velocity along U_{HS}.

values of the symmetric and non-symmetric shape of the stenosis. Velocities increase as stenosis length increases. Further, velocity is lowest at the center and increases along the walls. Velocity increases with an increase in stenosis length. The velocity increases in magnitude due to the narrowing of the channel as δ_l increases. At the same time, the velocity decreases as it approaches the walls when there are numerous stenoses. Figure 2c will discuss velocity behavior in the case of EOF, a basic theory of the Stokes equation. In this case, the variation of the electro-osmosis (m) velocity at the center is a minimum and increases gradually along the walls of the stenosis. By increasing the electro-osmosis parameter velocity. It is the movement of liquid generated by an applied voltage through a porous material, capillary tube, membrane, micro-channel, or any other fluid conduit known as EOF or electro-osmosis. EOF has minimal influence on channel characteristics since it is unaffected by the conduit size because electro-osmotic velocities are independent of conduit size. When EOF occurs in tiny channels, it has the most significant impact. Capillary electrophoresis relies heavily on EOF, a crucial component of chemical separation processes. A buffered solution, as well as unfiltered water, may experience EOF. In Figure 2d, the volumetric flow Q's effect teaches us about liquid flow in various variations; the velocity of the volumetric flow is lowest in the center and rapidly increases along the channel walls. Figure 2e will discuss the behavior of the Helmholtz-Smoluchowski parameter U_{HS} at four different variations. The velocity at the center is minimum and increases along the channel walls as the Helmholtz-Smoluchowski parameter velocity increases. In addition, the value of velocity is at its peak when U_{HS} is equal to zero, and it steadily decreases as the value of U_{HS} increases. Therefore, an electric field applied axially is the primary mechanism that may be used to control the flow rate. These velocity graphs show that the rise in velocity is lower for

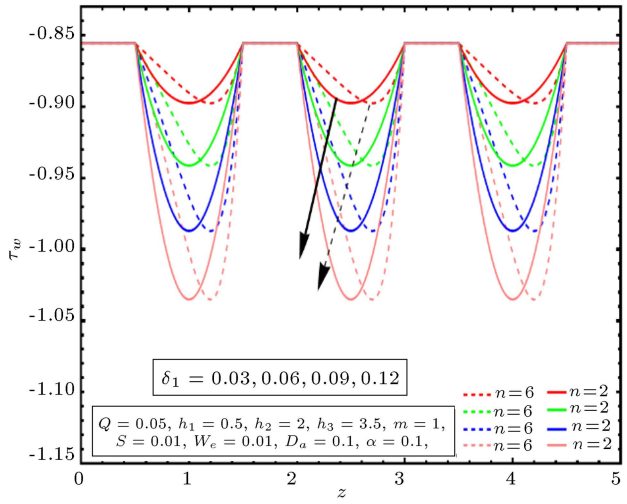

Figure 3a. stress along δ_l.

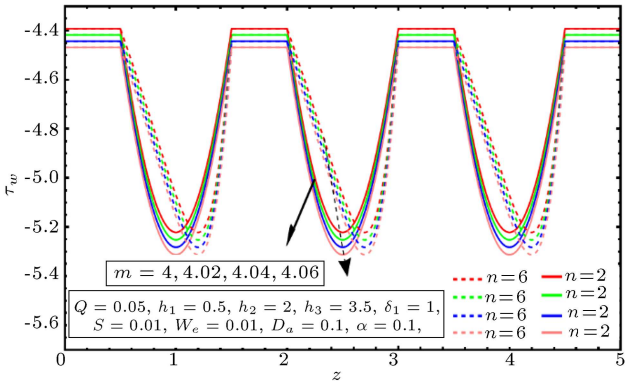

Figure 3b. stress along m.

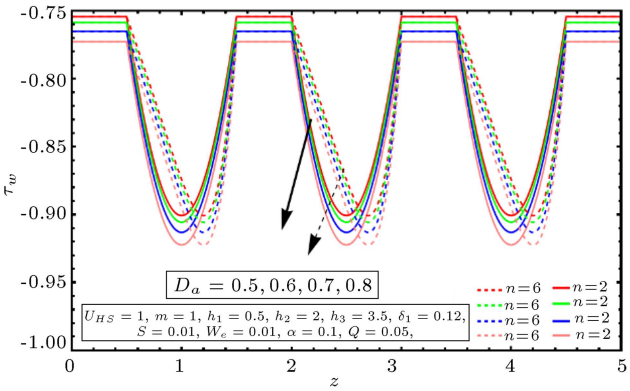

Figure 3c. stress along D_α.

non-uniform shapes compared to uniform shapes of numerous stenoses. This may be noticed by comparing the two types of shapes. In Figure 3a–3e, we will discuss shear stress behavior for various increasing parameters. Shear stress is the ratio of applied force to the cross-sectional area; increasing the cross-sectional area decreases shear stress. Plots of the shear stresses at walls that have numerous stenosis. Figure 3a illustrates the behavior of stenosis length for four different values. As taking an increment in the values

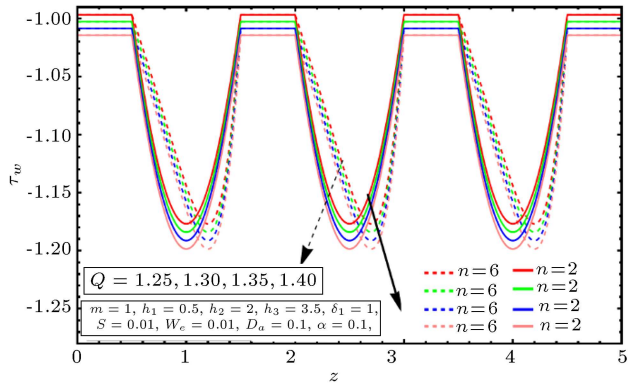

Figure 3d. stress along Q.

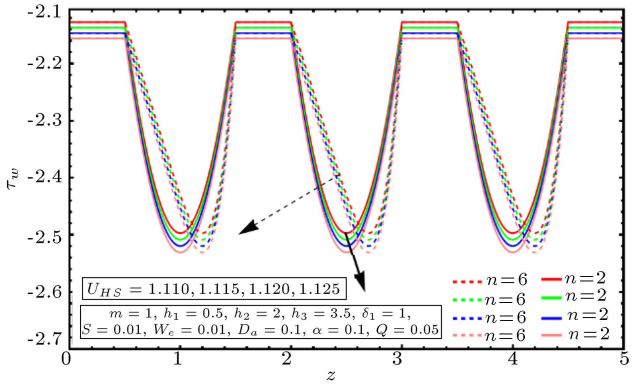

Figure 3e. stress along U_{HS}.

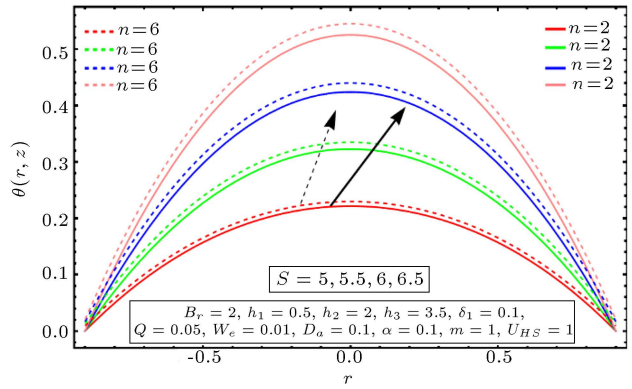

Figure 4a. Temperature along S.

of stenosis length, the shear stress decreases as shown in the figure here, the symmetric shape of multiple stenoses at $n = 2$ and the non-symmetric shape of multiple stenoses at $n = 6$. In Figure 3b, increasing the values of the electroosmotic parameters decreases the stress rate. In Figure 3c, with an increase in the values of Darcy number, shear stress is decreasing, and it decreases the porosity of the medium. In Figure 3d, the increment in the volumetric flow rate decreases the shear stress. Figure 3e discusses the behavior of the Helmholtz-Smoluchowski parameter, as its increasing values result in a decline in shear stress.

Figures 4a–4f shows temperature graphs, each

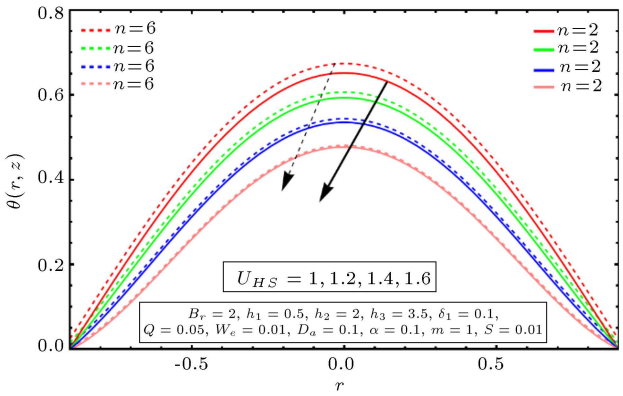

Figure 4b. Temperature along U_{HS}.

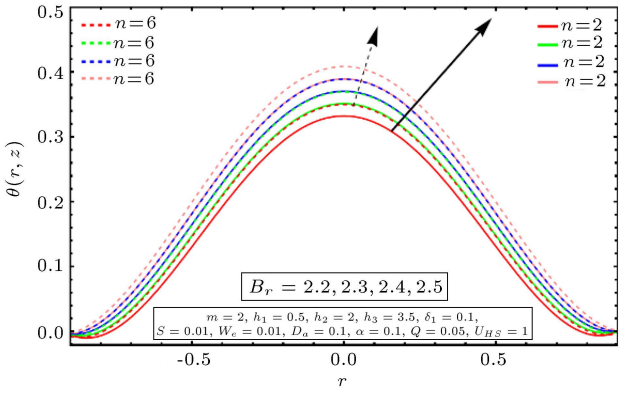

Figure 4c. Temperature along Br.

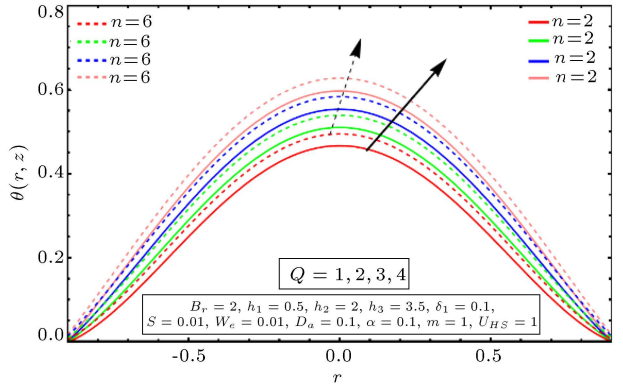

Figure 4d. Temperature along Q.

representing a different value for the related parameters. Figure 4a discusses the effect of the Joule heating parameter (the generation of heat by blood flow through arteries is referred to as Joule heating), resistive heating, or Ohmic heating. All of these names refer to the same phenomenon. Figure 4b shows the behavior of the parameter Helmholtz-Smoluchowski velocity that decreases the temperature with an increase in the values of Helmholtz-Smoluchowski velocity, and Figure 4c reveals that increasing the values of the Brickman number temperature profile increases the temperature. It is also increased due to heat transport

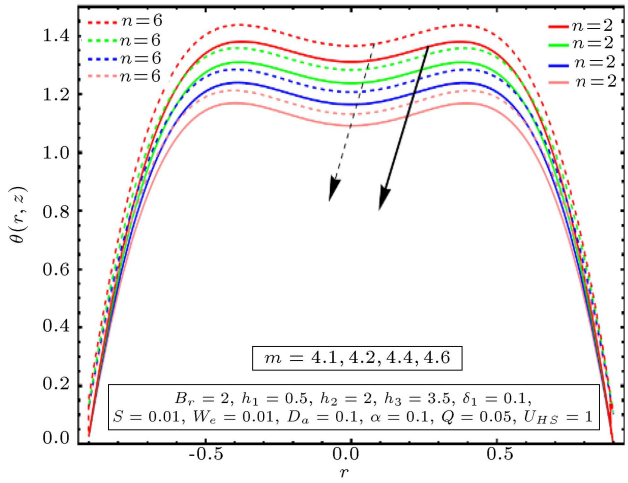

Figure 4e. Temperature along m.

by molecular conduction. Figure 4d shows that the channel's temperature decreases as the volumetric flow rate increases. So, from the graphs, it is clear that the temperature has lower values for symmetric $n = 2$ shapes than the antisymmetric $n = 6$ shapes of the multiple stenoses. Figure 4e shows the behavior of the electro-osmotic parameter, showing that the temperature decreases with increasing values of the electro-osmotic parameter. The temperature rises more quickly for this. All of these temperature graphs show that the increase in temperature for multiple stenoses with a uniform shape is greater than the increase in temperature for multiple stenoses with a non-uniform shape. In addition, a decrease in temperature and velocity is seen when there is an increase in the axial electric field. Because of this, electro-osmosis can be used to change the flow's speed and temperature as needed.

The streamlines representing the flow rate Q are also shown in Figure 5a–5d. When several stenoses have a symmetric form, there is an increase in the size of the trap with each successively higher Q. When the form, however, is not symmetrical, the size of the trapping area shrinks in response to an increase in Q. In addition, if the form of the multiple stenoses is symmetric, then the trapping pattern's shape will also be symmetric. However, if the shape of the multiple stenoses is non-symmetric, then the trapping pattern will have a non-symmetric shape. The streamline graphs in Figure 6a–6d are for increasing values of the electro-osmosis parameter m, and they consider both symmetric and non-symmetric multiple stenoses geometries. As m increases, the trapping size decreases, indicating symmetric stenosis. For the non-symmetric scenario, however, there is an increase in the magnitude of the trapped streamlines. Furthermore, the walls with numerous stenosis may be seen quite well in these streamlines. In addition to this, both symmetric and non-symmetric forms may be seen quite well.

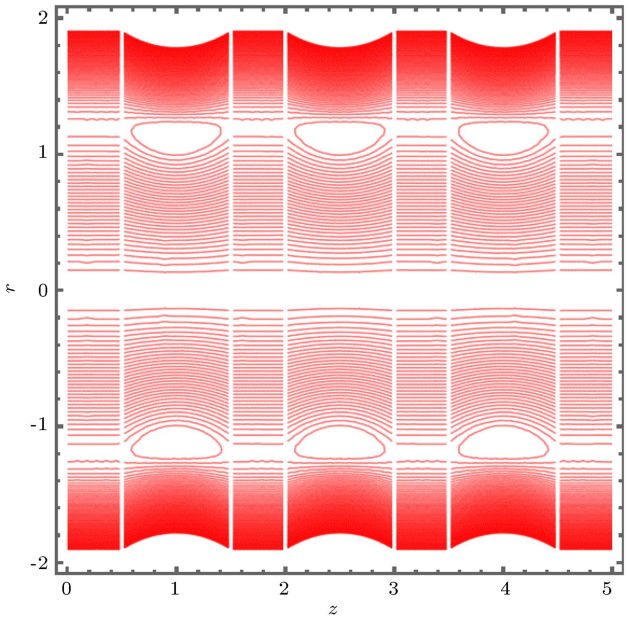

Figure 5a. Streamline $Q = 1$, $n = 2$.

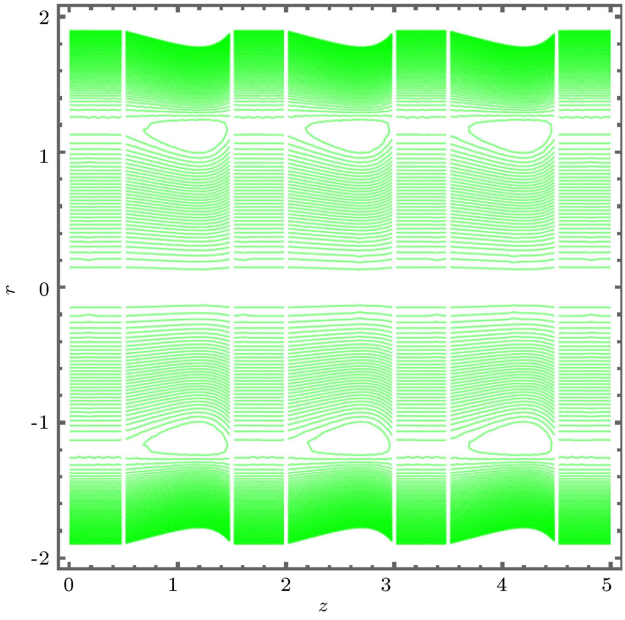

Figure 5c. Streamline $Q = 1$, $n = 6$.

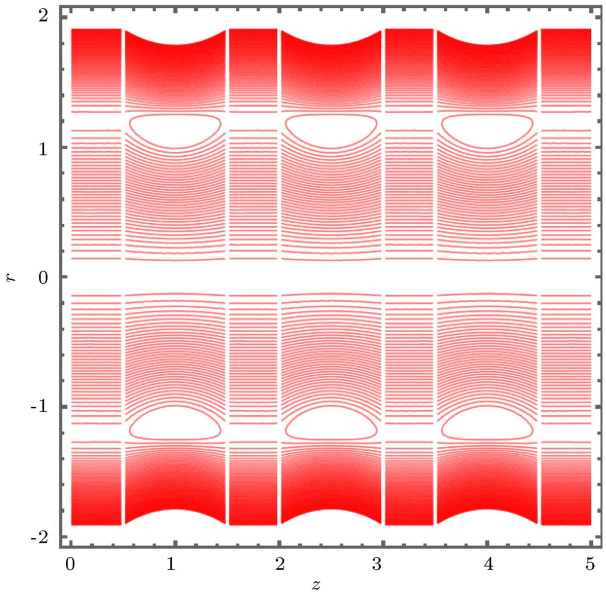

Figure 5b. Streamline $Q = 2$, $n = 2$.

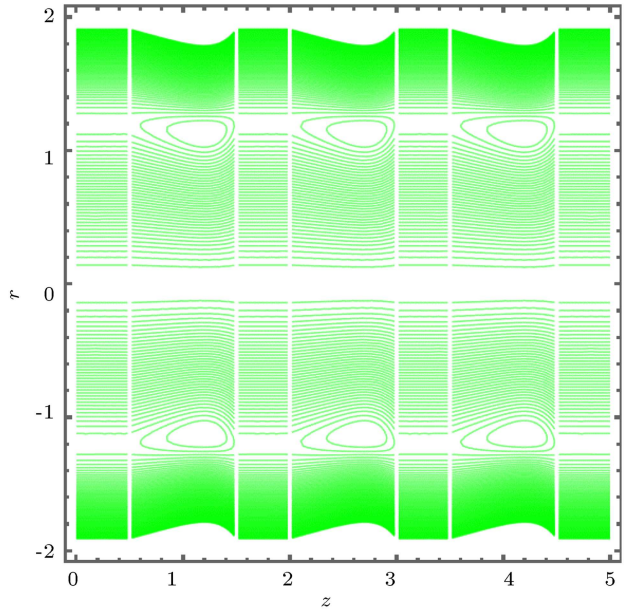

Figure 5d. Streamline $Q = 2$, $n = 6$.

5. Conclusion

Williamson's fluid model has made it a tedious task to find the solution, and it is not easy to handle the solution by an exact method to find an approximate solution, such as the Homotopy perturbation solution. The main findings are listed below:

- The limitation of this work is that it was done without using any laboratory frame. The whole work is analytical, so only some suppositions about this work are suggested;
- There are many merits, but here are a few defined; they can be used for the medication process and treatment of sickle cells using electro-osmosis;
- A parabolic hemodynamic profile is observed for the velocity case, but temperature distribution is not parabolic in all parameter cases;
- Such models help locate stenosis, drug delivery, medication, and surgical procedures;
- This work will prove a benchmark problem for the study of further hemodynamic models;
- This work concludes that regular smoking results in stenosis; sugar also develops stenosis like high

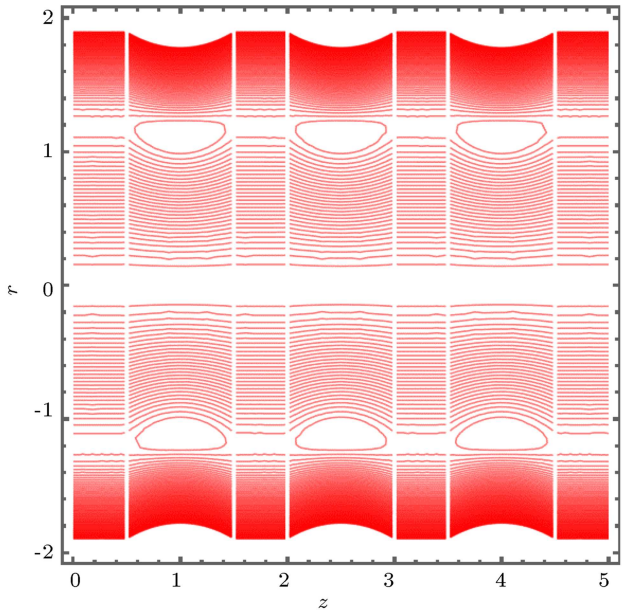

Figure 6a. Streamline $m = 2$, $n = 2$.

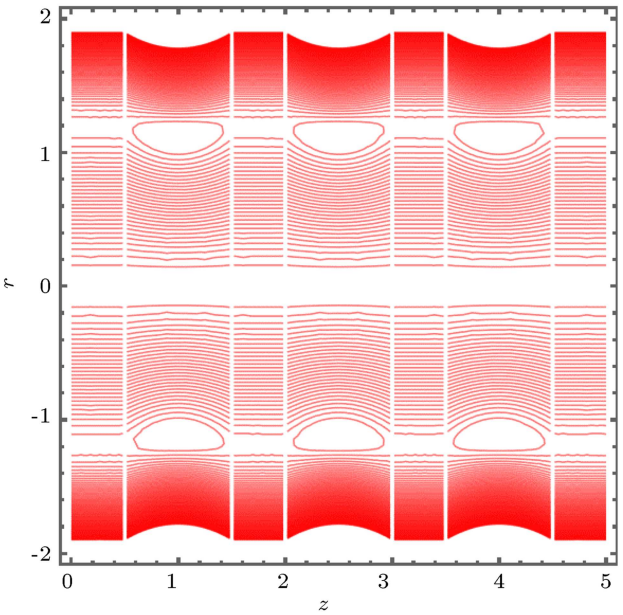

Figure 6b. Streamline $m = 3$, $n = 2$.

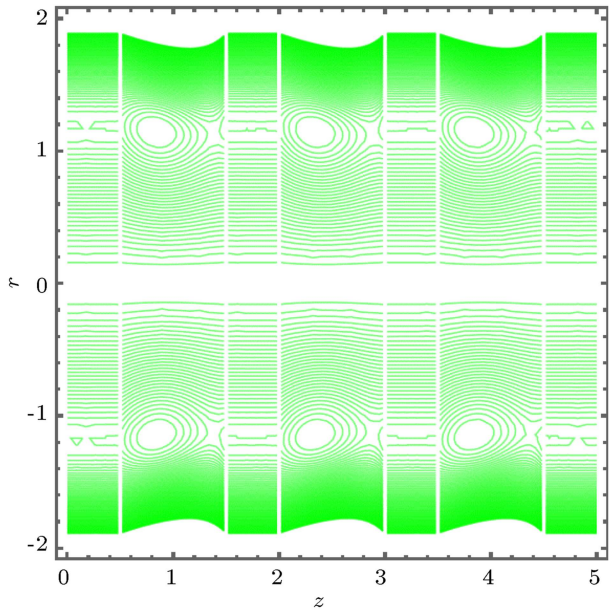

Figure 6c. Streamline $m = 2$, $n = 6$.

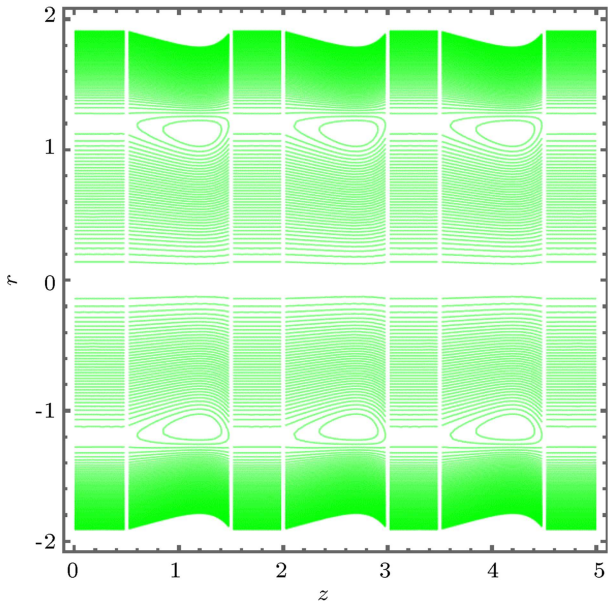

Figure 6d. Streamline $m = 3$, $n = 6$.

cholesterol, high blood pressure, diabetes, obesity, and injuries to vessel walls;

- Combining symmetric and non-symmetric stenosis formation is considered to deal with more realistic surgical problems;
- Homotopy perturbation method is utilized to solve this complicated problem, and a proper solution procedure is provided in the manuscript to handle such complex mathematical models mathematically;
- Graphical illustrations are provided that perfectly match the mathematical solutions that satisfy the considered problem's boundary conditions;
- Exercise, surgery, treatment, carotid Angioplasty, and stenting can remove stenosis;
- In the case of the streamlines, the multiple shapes of the symmetric stenosis are also symmetric in the case of trapping, but when we deal with the antisymmetric shape of the multiple stenoses, it is antisymmetric in the case of trapping.

Nomenclature

v, u	Radial and axial velocity components
B_r	Brickman number

S	Joule heating parameter
e	Electronic charge
T^*	Average temperature of electrolyte solution
U_{HS}	Helmholtz-Smoluchowski velocity
ρ_e	Density of total ionic charge
δ_l^*	Maximum height of stenosis in the dimensional form
E_z	Axial electrical field
m	Electro-osmotic parameter
ζ	Zeta potential
I_e	Current density
s_l	Electro-kinetic potential function stenosis Length ($l = 1, 2, 3$)
$n = 2$	Symmetric shape of multiple stenoses
$n = 6$	Non-symmetric shape of multiple stenoses
n^+, n^-	Cation and anion densities
z^*	Charge balance
r, z	Cylindrical coordinate system
$n \geq 2$	Multiple stenoses shape parameter
E	Permittivity
d_l	Stenosis position ($l = 1, 2, 3$)
R	Non-stenotic radius of artery
K_B	Boltzmann Constant
σ_e	Electrical resistivity of fluid
n_0	Ions concentration
W_e	Weissenberg number

References

1. Huang, X., Gordon, M.J., and Zare, R.N. "Current-monitoring method for measuring the electroosmotic flow rate in capillary zone electrophoresis", *Analytical Chemistry*, **60**(17), pp. 1837–1838 (1988).
2. Minerick, A.R., Ostafin, A.E., and Chang, H.C. "Electrokinetic transport of red blood cells in microcapillaries", *Electrophoresis,* **23**(14), pp. 2165–2173 (2002).
3. Dolník, V., Liu, S., and Jovanovich, S. "Capillary electrophoresis on microchip", *Electrophoresis: An International Journal*, **21**(1), pp. 41–54 (2000).
4. Wu, R.C. and Papadopoulos, K.D. "Electroosmotic flow through porous media: Cylindrical and annular models", *Colloids and Surfaces A: Physicochemical and Engineering Aspects*, **161**(3), pp. 469–476 (2000).
5. Yang, R.J., Fu, L.M., and Lin, Y.C. "Electroosmotic flow in microchannels", *Journal of Colloid and Interface Science*, **239**(1), pp. 98–105 (2001).
6. Zhao, C. and Yang, C. "An exact solution for electro-osmosis of non-newtonian fluids in microchannels", *Journal of Non-Newtonian Fluid Mechanics*, **166**(17–18), pp. 1076–1079 (2011).
7. Tang, G.H., Li, X.F., He, Y.L., et al. "Electroosmotic flow of non-Newtonian fluid in microchannels", *Journal of Non-Newtonian Fluid Mechanics,* **157**(1–2), pp. 133–137 (2009).
8. Liu, Q., Jian, Y., and Yang, L. "Alternating current electroosmotic flow of the Jeffreys fluids through a slit microchannel", *Physics of Fluids,* **23**(10), 102001 (2011).
9. Nadeem, S., Kiani, M.N., Saleem, A., et al. "Microvascular blood flow with heat transfer in a wavy channel having electroosmotic effects", *Electrophoresis*, **41**(13–14), pp. 1198–1205 (2020).
10. Narla, V.K. and Tripathi, D. "Electro-osmosis modulated transient blood flow in curved microvessels: A study of a mathematical model", *Microvascular Research*, **123**, pp. 25–34 (2019).
11. Tripathi, D., Yadav, A., Bég, O.A., et al. "Study of microvascular non-Newtonian blood flow modulated by electro-osmosis", *Microvascular Research,* **117**, pp. 28–36 (2018).
12. Akram, J., Akbar, N.S., and Maraj, E.N. "A comparative study on the role of nanoparticle dispersion in electro-osmosis-regulated peristaltic flow of water", *Alexandria Engineering Journal*, **59**(2), pp. 943–956 (2020).
13. Saleem, S., Akhtar, S., Nadeem, S., et al. "Mathematical study of electroosmotically driven peristaltic flow of Casson fluid inside a tube having systematically contracting and relaxing sinusoidal heated walls", *Chinese Journal of Physics,* **71**, pp. 300–311 (2021).
14. Ponalagusamy, R. "Blood flow through stenosed tube", Ph.D Thesis, Indian Institute of Technology Bombay (1986).
15. Ponalagusamy, R. "Blood flow through an artery with mild stenosis: A two-layered model, different shapes of stenoses and slip velocity at the wall", *Journal of Applied Sciences,* **7**(7), pp. 1071–1077 (2007).
16. Varshney, G., Katiyar, V., and Kumar, S. "Effect of magnetic field on the blood flow in an artery having multiple stenoses: A numerical study", *International Journal of Engineering, Science, and Technology*, **2**(2), pp. 967–82 (2010).
17. Nadeem, S. and Ijaz, S. "Single wall carbon nanotube (SWCNT) examination on blood flow through a multiple stenosed artery with variable nanofluid viscosity", *AIP Advances*, **5**(10), 107217 (2015).
18. Haider, J.A. and Ahmad, S. "Dynamics of the Rabinowitsch fluid in a reduced form of elliptic duct using finite volume method", *International Journal of Modern Physics*, B, **36**(30), 2250217 (2022).
19. Akbar, N.S., Nadeem, S., and Ali, M. "Jeffrey fluid model for blood flow through a tapered artery with a stenosis", *Journal of Mechanics in Medicine and Biology,* **11**(03), pp. 529–545 (2011).
20. Akbar, N.S. and Nadeem, S. "Simulation of heat and chemical reactions on Reiner Rivlin fluid model for blood flow through a tapered artery with stenosis", *Heat and Mass Transfer*, **46**(5), pp. 531–539 (2010).

21. Haider, J.A., Asghar, S., and Nadeem, S. "Travelling wave solutions of the third-order KdV equation using Jacobi elliptic function method", *International Journal of Modern Physics*, B, **37**(12), 2350117 (2023).
22. Toghraie, D., Esfahani, N.N., Zarringhalam, M., et al. "Blood flow analysis inside different arteries using non-Newtonian Sisko model for application in biomedical engineering", *Computer Methods and Programs in Biomedicine*, **190**, 105338 (2020).
23. Yan, S.R., Zarringhalam, M., Toghraie, D., et al. "Numerical investigation of non-Newtonian blood flow within an artery with cone shape of stenosis in various stenosis angles", *Computer Methods and Programs in Biomedicine*, **192**, 105434 (2020).
24. Riaz, A., Bobescu, E., Ramesh, K., et al. "Entropy analysis for cilia-generated motion of Cu-blood flow of nanofluid in an annulus", *Symmetry*, **13**(12), 2358 (2021).
25. Tripathi, D., Prakash, J., Tiwari, A.K., et al. "Thermal, microrotation, electromagnetic field, and nanoparticle shape effects on Cu-CuO/blood flow in microvascular vessels", *Microvascular Research*, **132**, 104065 (2020).
26. Shehzad, N., Zeeshan, A., and Ellahi, R. "Electroosmotic flow of MHD power law Al_2O_3-PVC nanofluid in a horizontal channel: Couette-Poiseuille flow model", *Communications in Theoretical Physics*, **69**(6), p. 655 (2018).
27. Bhatti, M.M., Arain, M.B., Zeeshan, A., et al. "Swimming of gyrotactic microorganism in MHD Williamson nanofluid flow between rotating circular plates embedded in a porous medium: Application of thermal energy storage", *Journal of Energy Storage*, **45**, 103511 (2022).
28. Ouellette, J., *An-Ti-Ci-Pa-Tion: The Physics of Dripping Honey*, Scientific America (2013).
29. Williamson, R.V. "The flow of pseudoplastic materials", *Industrial & Engineering Chemistry*, **21**(11), pp. 1108–1111 (1929).
30. Khan, M., Malik, M.Y., Salahuddin, T., et al. "Heat and mass transfer of Williamson nanofluid flow yield by an inclined Lorentz force over a nonlinear stretching sheet", *Results in Physics*, **8**, pp. 862–868 (2018).
31. Khan, M., Salahuddin, T., Malik, M.Y., et al. "Change in viscosity of Williamson nanofluid flow due to thermal and solutal stratification", *International Journal of Heat and Mass Transfer*, **126**, pp. 941–948 (2018).
32. Khan, N.A., Khan, S., and Riaz, F. "Boundary layer flow of Williamson fluid with chemically reactive species using scaling transformation and homotopy analysis method", *Mathematical Sciences Letters*, **3**(3), p. 199 (2014).
33. Das, S., Pal, T.K., Jana, R.N., et al. "Significance of Hall currents on hybrid nano-blood flow through an inclined artery having mild stenosis: Homotopy perturbation approach", *Microvascular Research*, **137**, 104192 (2021).
34. Ahmad, I. and Ilyas, H. "Homotopy perturbation method for the nonlinear MHD Jeffery-Hamel blood flows problem", *Applied Numerical Mathematics*, **141**, pp. 124–132 (2019).
35. Hamrelaine, S., Mebarek-Oudina, F., and Sari, M.R. "Analysis of MHD Jeffery Hamel flow with suction/injection by homotopy analysis method", *Journal of Advanced Research in Fluid Mechanics and Thermal Sciences*, **58**(2), pp. 173–186 (2019).
36. Sudha, T., Umadevi, C., Dhange, M., et al. "Effects of stenosis and dilatation on flow of blood mixed with suspended nanoparticles: A study using homotopy technique", *International Journal of Applied Mechanics and Engineering*, **26**(1), pp. 251–265 (2021).
37. Tripathi, B. and Sharma, B.K. "Effect of variable viscosity on MHD inclined arterial blood flow with chemical reaction", *International Journal of Applied Mechanics and Engineering*, **23**(3), pp. 767–785 (2018).
38. Ullah, I., Hayat, T., Alsaedi, A., et al. "Modeling for radiated Marangoni convection flow of magneto-nano liquid subject to activation energy and chemical reaction", *Scientia Iranica*, **27**(6), pp. 3390–3398 (2020).
39. Makinde, O.D. and Gnaneswara Reddy, M. "MHD peristaltic slip flow of Casson fluid and heat transfer in channel filled with a porous medium", *Scientia Iranica*, **26**(4), pp. 2342–2355 (2019).
40. Kaveh, A. and Kooshkebaghi, M. "Artificial coronary circulation system: A new bio-inspired metaheuristic algorithm", *Scientia Iranica*, **26**(5), pp. 2731–2747 (2019).
41. Akhtari, H., Mirzaee, I., and Pourmahmoud, N. "Lattice Boltzmann simulation of blood flow properties and vessel geometry in open and closed vessels: A numerical study", *Scientia Iranica*, **26**(6), pp. 3283–3292 (2019).
42. Basar, A., Kabak, Ö., and Topcu, Y.I. "A tabu search algorithm for a multi-period bank branch location problem: A case study in a Turkish bank", *Scientia Iranica*, **26**(6), pp. 3728–3746 (2019).
43. Tang, L.N., Ma, Y.Z., Wang, J.J., et al. "Robust parameter design of supply chain inventory policy considering the uncertainty of demand and lead time", *Scientia Iranica*, **26**(5), pp. 2971–2987 (2019).
44. Sohrabi, M., Zandieh, M., and Afshar-Nadjafi, B. "An equity-oriented multi-objective inventory management model for blood banks considering the patient condition: a real-life case", *Scientia Iranica*, pp. 1–39 (2021).
45. Fallahi, H., Shirani, E., and Zohravi, E. "Hemodynamic analysis of coronary artery bypass grafting with elastic walls and different stenoses", *Scientia Iranica*, **28**(2), pp. 773–784 (2021).
46. Gitinavard, H., Ghodsypour, S.H., and Akbarpour Shirazi, M. "A bi-objective multi-echelon supply chain model with Pareto optimal points evaluation for perishable products under uncertainty", *Scientia Iranica*, **26**(5), pp. 2952–2970 (2019).

47. Hamdi-Asl, A., Amoozad-Khalili, H., Tavakkoli-Moghaddam, R., et al. "Toward sustainability in designing agricultural supply chain network: A case study on palm date", *Scientia Iranica*, pp. 1–27 (2021).

48. Liu, X., Chen, X., Zhang, Y., et al. "The thermal behavior of blood flow in the arteries with various radii and various stenosis angles using non-Newtonian Sisko model", *Alexandria Engineering Journal*, **61**(9), pp. 7195–7201 (2022).

49. Cherkaoui, I., Bettaibi, S., Barkaoui, A., et al. "Magnetohydrodynamic blood flow study in stenotic coronary artery using lattice Boltzmann method", *Computer Methods and Programs in Biomedicine*, 106850 (2022).

50. Carvalho, V., Lopes, D., Silva, J., et al., *Comparison of CFD and FSI Simulations of Blood Flow in Stenotic Coronary Arteries* (2022).

51. Ellahi, R., Sait, S.M., Shehzad, N., et al. "A hybrid investigation on numerical and analytical solutions of electro-magnetohydrodynamics flow of nanofluid through porous media with entropy generation", *International Journal of Numerical Methods for Heat & Fluid Flow*, **30**(2), pp. 834–854 (2019).

52. Bakker, L.M.M.L., Xiao, N., Van De Ven, A.A.F., et al. "Image-based blood flow estimation using a semi-analytical solution to the advection-diffusion equation in cylindrical domains", *Journal of Fluid Mechanics*, **924**, pp. 924A18-1–924A18-11 (2021).

53. Μανώλης, Θ.Δ and Κουτσούκος, Θ. "Simulation of micropolar fluid flows: Validation of numerical results with analytical solutions" Bachelor's Thesis (2018).

54. Ramesh, K., Tripathi, D., Bég, O.A., et al. "Slip and hall current effects on Jeffrey fluid suspension flow in a peristaltic hydromagnetic blood micropump", *Iranian Journal of Science and Technology, Transactions of Mechanical Engineering*, **43**(4), pp. 675–692 (2019).

55. Zhang, L., Bhatti, M.M., and Michaelides, E.E. "Thermally developed coupled stress particle-fluid motion with mass transfer and peristalsis", *Journal of Thermal Analysis and Calorimetry*, **143**(3), pp. 2515–2524 (2021).

56. Raje, A., Devakar, M., and Ramgopal, N.C. "Influence of heat transfer on the flow of immiscible fluids through pipes: An analytical study", *Journal of Porous Media*, **24**(11), pp. 85–99 (2021).

57. Bai, H.G., Jeyanthi, M.P., Hemavathy, P., et al. "Blood flow in arteries with stenoses: A three-dimensional unsteady flow", *Journal of Positive School Psychology*, **6**(2), pp. 3336–3343 (2022).

58. Saleem, A., Akhtar, S., and Nadeem, S. "Biomathematical analysis of electro-osmotically modulated hemodynamic blood flow inside a symmetric and nonsymmetric stenosed artery with joule heating", *International Journal of Biomathematics*, **15**(02), 2150071 (2022).

59. Shao, S. and Sun, Q. "Evaluation of intracranial artery stenosis using time-of-flight magnetic resonance angiography: New wine in an old bottle", *European Radiology*, **32**(6), pp. 1–2 (2022).

60. Kamangar, S. "Influence of multi stenosis on hemodynamic parameters in an idealized coronary artery model", *Journal of Applied Fluid Mechanics*, **15**(1), pp. 15–23 (2022).

61. Jamali, M.S.A. and Ismail, Z. "Generalized power law model of blood flow in a stenosed bifurcated artery", *Annals of Mathematical Modeling*, **1**(2), pp. 35–46 (2022).

62. Akhtar, S., McCash, L.B., Nadeem, S., et al. "Mechanics of non-Newtonian blood flow in an artery having multiple stenoses and electroosmotic effects", *Science Progress*, **104**(3), 00368504211031693 (2021).

63. Mekheimer, K.S., Haroun, M.H., and Elkot, M.A. "Effects of magnetic field, porosity, and wall properties for anisotropically elastic multi-stenosis arteries on blood flow characteristics", *Applied Mathematics and Mechanics*, **32**(8), pp. 1047–1064 (2011).

64. Liechty, B.C., Webb, B.W., and Maynes, R.D. "Convective heat transfer characteristics of electro-osmotically generated flow in microtubes at high wall potential", *International Journal of Heat and Mass Transfer*, **48**(12), pp. 2360–2371 (2005).

65. Akbar, N.S. and Butt, A.W. "Entropy generation analysis in convective ferromagnetic nano blood flow through a composite stenosed arteries with permeable wall", *Communications in Theoretical Physics*, **67**(5), p. 554 (2017).

Biographies

Sohail Nadeem is Professor of Mathematics at Quaid-i-Azam University, Islamabad, Pakistan. His contribution to applied mathematics is recognized at a national and international level. He has supervised a notable number of PhD students. He is also the editor of several prestigious international journals.

Jamil Abbas Haider is a PhD scholar at the Department of Mathematics, Quaid-i-Azam University, Islamabad, Pakistan. His field of research is applied mathematics, computational fluid dynamics, and nonlinear dynamical systems. He is working under the supervision of Professor Sohail Nadeem. He also got his MPHIL in mathematics under the supervision of Dr. Saleem Asghar, a well-known Professor.

Salman Akhtar is a PhD research fellow at the Department of Mathematics, Quaid-i-Azam University, Islamabad. He has published many research articles under the supervision of Professor Nadeem.